J Mater Sci (2010) 45:6139–6150
DOI 10.1007/s10853-010-4700-4

Synergy in carbon black filled natural rubber nanocomposites. Part II: Abrasion and viscoelasticity in tire like applications

Mithun Bhattacharya · Anil K. Bhowmick

Received: 14 February 2010 / Accepted: 7 June 2010 / Published online: 22 June 2010

Abstract Synergistic effect of carbon black (CB) in presence of nanofillers (nanoclay and nanofiber) on mechanical and dynamic mechanical properties was discussed in light of electrostatic interactions and the concomitant microstructural developments, in Part I of this series. These interactions enhanced filler dispersion and ensured efficient stress transfer from the matrix resulting in improvement in properties, undiminished even by continual increase in CB loading. In this part, the micromechanical processes that influence wear behavior have been addressed conjointly with dynamic mechanical properties. Tribological characteristics were studied by sliding rubber wheel samples against a steel blade, in a specially designed abrader, in both transient and steady state conditions. Wear loss was reduced in the dual filler nanocomposites by 33% (over the CB microcomposite) in less stringent and 75% under severe wear conditions. These CB filled nanocomposites also illustrated lowering of coefficient of friction and temperature build-up. This was attributed to efficient heat dissipation due to the formation of a unique microstructural architecture by the participating fillers and also an adhering transfer film on the abraders' counterface. From viscoelastic measurements, the CB filled nanocomposites were also found to lie in the high performance window of good wet skid and low rolling resistance.

M. Bhattacharya · A. K. Bhowmick
Rubber Technology Center, Indian Institute of Technology, Kharagpur 721302, India
e-mail: bhatt.mithun@gmail.com

A. K. Bhowmick (✉)
Indian Institute of Technology, Patna 800013, India
e-mail: anilkb@rtc.iitkgp.ernet.in; director@iitp.ac.in

Introduction

Nanoclay and carbon nanofiber (CNF) reinforced polymers have been engineered and synthesized to form different advanced, novel functional materials targeted at different structural and technological applications. Unfortunately, the wear behavior of such nanocomposites has not received its due attention [1–3]. This may be due to their complex viscoelastic behavior which makes the processes and analysis very complicated. Tribological properties of polymers are known to improve with the addition of lubricating and/or reinforcing fillers [4]. Common examples of lubricating fillers are graphite, poly(tetrafluoroethylene) (PTFE), molybdenum disulfide (MoS_2), and some synthetic oils; while common reinforcing fillers include treated glass fibers, carbon fibers, etc. Amongst nanomaterials, Ti, Si, Zn, carbon nanotube (CNT) based materials have been studied and found to favorably influence the wear process of some polymers [5]. When it comes to rubbers, carbon blacks have for long been the material of choice with regard to property enhancements, wear resistance in particular [6]. However, the influence of nanofillers on these properties has not been extensively studied.

On reduction of size of particle inclusions from micro to the nano domain, several properties like mechanical, dynamic mechanical, barrier, thermal, electrical, optical, etc. have been found to improve drastically [7]. Although there is no direct dependence of wear rate on any one mechanical property, still the synergy demonstrated in terms of mechanical and dynamic mechanical properties of CB filled nanocomposites (Part I) may be expected to favorably influence their tribological behavior.

Wear behavior of nano filled thermoplastic [2, 8–16] and thermoset [17–22] resins have been reported to have encouraging results. Dasari et al. [1] studied the role of clay

on the sliding wear characteristics of nylon 6 nanocomposites and showed that exfoliation or homogenous dispersion of nanoparticles alone is insufficient to improve the wear resistance. Without very good bonding between clay layers and matrix, interfacial debonding occurs in addition to intra-gallery delaminations of the clay layers. Thus, it is imperative to improve the dispersion and interfacial interaction of the nanoparticles in polymers. It is surprising that only sparse wok is available in the field of elastomeric nanocomposites in wear resistant application. Gatos et al. [20] observed that the organoclay modified clay containing hydrogenated nitrile (HNBR) and ethylene/propylene/diene (EPDM) rubbers may exhibit low resistance to wear of rubbers, as the alignment of the clay platelets in planes parallel to the sliding direction may be disadvantageous. Karger-Kocsis and co-workers have studied CNF-modified santoprene thermoplastic elastomer [3] and HNBR/fluoroelastomer (FKM)/CNT compounds under dry sliding and fretting conditions against steel [21].

Thus, by following stringent dispersion processes and by ensuring strong rubber-filler interaction, the wear performance of rubber nanocomposites (RNCs) may also be expected to be significantly better than their micro counterparts. Furthermore, if used together, such a blend of nano and conventional filler (CB) systems may outclass the wear performance of each filler individually, by the formation of additional morphological structures.

The understanding of the mechanisms of wear is still in nascent stage and to improve the fundamental tribological knowledge of these novel materials, significant contributions are required. This report is a small attempt in that direction. In part II of this series, we explore the effect of CB loading on the abrasion resistance properties of the nanocomposites. The effect of nanofillers on the carbon black (CB) filled tire compositions has not been reported before. In this study, we have discussed the fundamentals of abrasion behavior of RNCs containing CB. We have treaded both the zones of transient (low wear) and steady state (high wear) abrasion. The differences in the wear dynamics and mechanisms under low and severe wear conditions have not been reported before; especially for CB filled RNCs which satisfy most specifications for tire like applications in terms of their mechanical and dynamic mechanical properties. This paper discusses the differences in behavior of micro- and nanocomposites of CB filled elastomeric formulations resembling those used in tire application. To the best of our knowledge, there is no such report in literature. Viscoelastic properties have for long been correlated to the wear behavior [22, 23]. However, for the first time, the implications of such viscoelastic behavior of CB filled RNCs on tire properties, like abrasion, wet skid and rolling resistance, have been reported here.

Table 1 Rubber formulation and order of mixing

Order of mixing	Ingredient	Loading in phr
1	Rubber	100.0
2	Nanoclay/nanofiber	4.0/6.0
3	Titanate	0.4/0.0[a]
4	Zinc oxide	5.0
5	Stearic acid	2.0
6	IPPD	1.0
7	Carbon black	50.0
8	Oil	5.0
9	CBS	0.8
10	Sulphur	2.0

[a] Nanofiber filled systems were process modified and did not contain titanate as modifier

Experimental

Materials used and the methodology utilized for preparing the nanocomposites have been listed in full detail in the previous paper (Part I). The recipe and order of mixing are tabulated in Table 1 and the sample designation is presented in the form of a flow chart which also is the schematic of the present work (Scheme 1).

The scheme also explains the sample designation used, for instance, the base CNF compound (having 6 phr loading) is represented as NF-6 and its nanoclay counter part (having 4 phr clay loading) is represented as NC-4, gum rubber is designated as R-0. The CBs are represented as follows, N2 (for N220), N3 (for N330) and N5 (for N550). The number immediately following the '-' is the phr loading of CB. For instance, NF-6/N5-30 refers to the CNF nanocomposite filled with 30 phr of N550. Similarly, NC-4/N3-30 represents 4 phr nanoclay loaded NR mixed with 30 phr of N330. The control is represented as R-0/N3-50, suggesting that it is the rubber compound devoid of

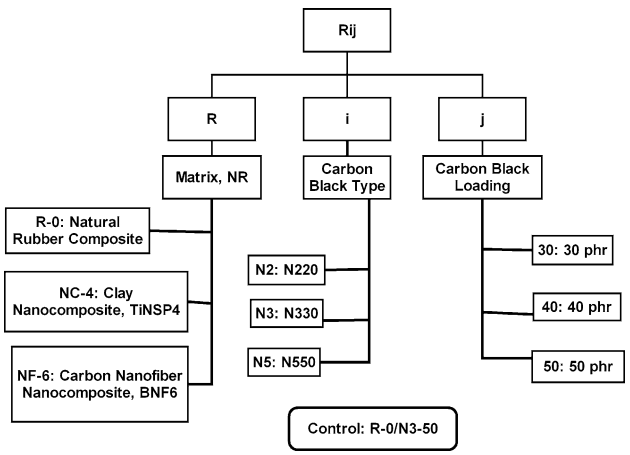

Scheme 1 Schematic of the work and sample designations

either nanoclay/nanofiber (0) and filled with 50 phr of N330. The basic recipe was kept common for all the systems. There was no variation in the loading of anti-oxidant, curatives, and cure accelerators.

Preparation of rubber specimen and experimental set-up and design

The rubber specimens as shown in Fig. 1a were prepared by molding in a David-Bridge hydraulic press (supplied by Castleton, Rocchdle, England) at a pressure of 5 MPa at 150 °C. To accommodate for the thickness and the metal insert, curing was performed till twice the t_{90} value (optimum cure time) obtained from a Monsanto oscillating disc rheometer (ODR-100s). The specimens were conditioned at room temperature for 16 h before carrying out the testing.

The new apparatus (Fig. 1b) designed for isolating the normal and tangential frictional force generated during rubber abrasion has been explained in detail elsewhere [24, 25]. Tests were performed by rotating a circular rubber disc against a rigidly held razor blade under different magnitudes of applied normal load, sliding speeds and time. Microtome blades (High Profile-Personna Plus, American Safety Razor Company, Staunton, USA) used as abrader were supplied by Personna U.K. Ltd., Nottinghamshire, UK. Only the outline of the apparatus and experimental procedure is described below.

Different weights were mounted on the hanger of the cantilever beam and the corresponding normal force exerted and the frictional force generated were grabbed from the dynamometer using an external circuit, amplified and projected onto a computer attached with the machine. During testing, the razor blade sticks to the rubber surface until there is a sudden break as a result of the gradually increasing pull which causes a very rapid slip. The blade sticks again and the process is repeated indefinitely and thus the resulting frictional force is not constant. This characteristic of abrasion of rubber by blade type abrader is called stick–slip motion (Fig. 2). Fukahori and Yamazaki [26] have also earlier emphasized the role of microvibrations and stick–slip motion in determining wear characteristics.

To obviate the effect of changing abrading capabilities of the razor blade, due to the wearing out of the inherent protective layer with run time, the blade was changed after every two runs. Frequent brushing was done to remove the debris particle from clinging onto the surface and the wear debris particles were collected from the wake zone of the experiment. The brushing was done in accord with the available literature [24, 25] by holding the soft polymeric bristles tangentially to the rotating wheel surface to ensure no drag force is imparted which could contribute towards abrasion.

Wear studies were carried out in accord with the orthogonal Taguchi design at room temperature and the weight loss and the temperature of the abraded surface of the rubber samples were measured. The amount of wear was measured as weight loss before and after abrasion and subsequently converted to volume loss. The temperature developed at the rubbing interface was measured with a non-contact infrared thermometer (Model MT-10, Metravi, Kolkata, India). The dynamic coefficient of friction (μ), frictional work (F_w), and abrasion loss (V) were computed from the primary observations.

Taguchi technique, a powerful tool for design of high quality systems based on orthogonal array experiments that provide much reduced variance for experiments, has been used in our earlier report for optimizing the process control parameters and quantifying their effects during the abrasion of RNCs [25]. Number of factors can control abrasion of rubbery materials, but the most prominent amongst them have been found to be (a) filler loading, (b) applied normal load, (c) speed, and (d) time of testing. These four factors were considered as main design factors in the present study, and optimization was achieved using predesigned

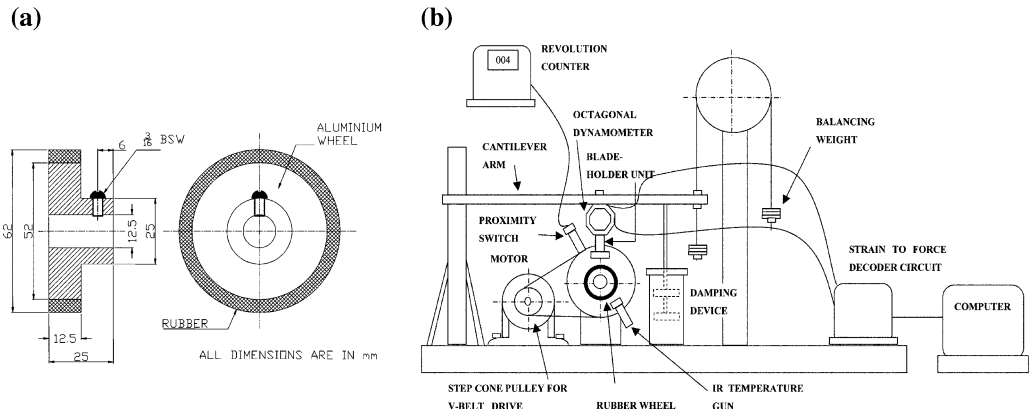

Fig. 1 **a** Rubber wheel sample and **b** schematic representation of the abrader machine

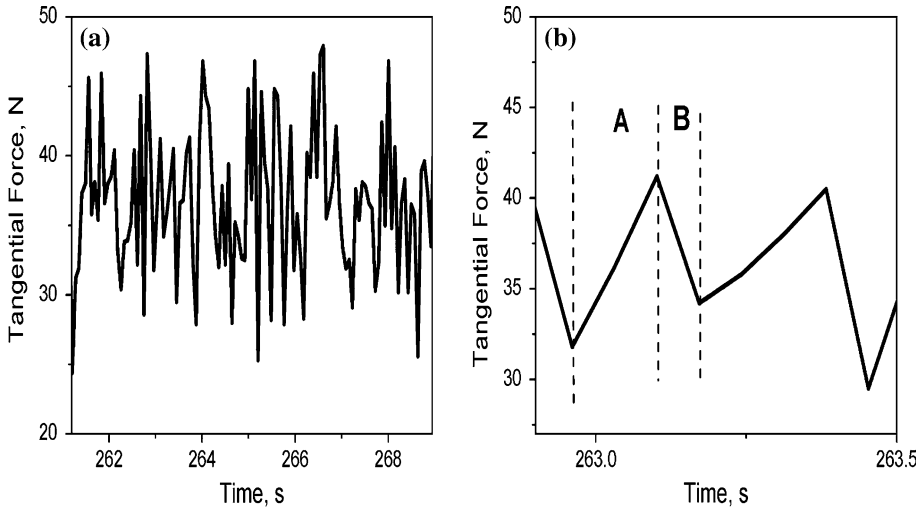

Fig. 2 Stick–slip motion; Zone *A* Stick, Zone *B* Slip

L25 orthogonal array (based on Taguchi method) having the above four parameters at five levels for each parameter. The primary response variable used to accomplish the present study was the volume loss. Abrasion studies on the dual filler containing nanocomposites have been done at those optimized conditions (Low wear: 50 g, 10 rpm, 5 min), as well as at the severe most conditions which correspond to the lowest abrasion resistance (high wear: 250 g, 50 rpm, 25 min). The low and high wear conditions correspond to unsteady and steady state abrasion, respectively. Thus, they happen to represent the two ends of the performance spectrum.

Studies on abraded surface and wear debris

The nature of abraded surfaces and the particulate and structured wear debris of each and every nanocomposite were collected on a clean paper for studying with an optical microscope (WILD M8, Wild Heerbrugg, Switzerland). The images were captured using Moticam1000, Motic China Group Co. Ltd., Xiamen, China. ImageJ software developed by the National Institutes of Health (USA) was extensively used for the purpose of image analysis. The results given here are the average of six samples. The standard deviations for perimeter, feret diameter, and roughness for these sets of observations are ±0.6, ±0.14, and ±6.1, respectively.

Dynamic mechanical thermal analysis (DMTA)

The dynamic mechanical spectra of the gum and RNCs were obtained by using a DMTA IV (Rheometric Scientific, NJ, USA) dynamic mechanical thermal analyzer. The sample specimens were analyzed in tensile mode at a constant frequency of 1 Hz, a strain of 0.01%, over a temperature range from −90 to 80 °C, at a heating rate of 2 °C/min. The data was analyzed by RSI Orchestrator application software. Storage modulus (E'), loss modulus (E''), and loss tangent (tan δ) were measured as function of temperature for all the samples under identical conditions. The temperature corresponding to the peak in tan δ versus temperature plot was taken as the glass–rubber transition temperature (T_g). The T_g has been reported along with the tan δ values at T_g, 0, and 60 °C. The latter two are known to correspond to the wet skid resistance and the rolling resistance, respectively, of rubber compounds engaged in tire applications.

Results and discussion

Abrasion

Relations between the volume loss and the frictional work and normal pressure for black filled nanocomposites are shown in Fig. 3. Figure 3a, b depicts the dependence of wear loss on applied normal pressure, while Fig. 3c, d illuminates the effect of frictional work on the same. As indicated in the figures, Fig. 3a and c corresponds to the high wear condition, while Fig. 3b and d are their low wear condition counterparts. The resulting power law parameters are reported in Table 2. The clay and fiber subheadings in Table 2 are self explanatory, while the general (GEN) category represents the two nanofillers averaged and then expressed as a single entity. It may thus be considered to be more representative of the family of nanofillers. It may be noted here that abrasion studies on the dual filler nanocomposites have been done at the two ends of the performance spectrum, that is low wear (50 g, 10 rpm, 5 min) and high wear (250 g, 50 rpm, 25 min). Wear rate when plotted against the frictional work input per unit revolution (and also normal pressure) in logarithmic scales is known

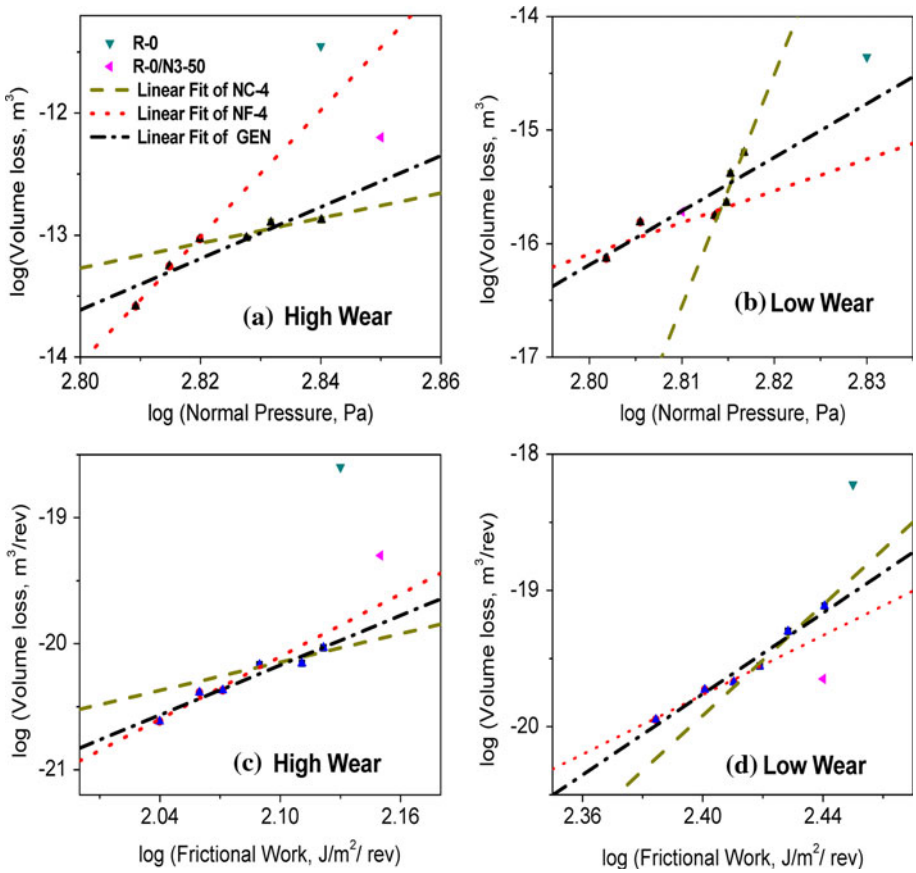

Fig. 3 Dependence of volume loss on normal pressure in **a** high wear and **b** low wear condition and also on frictional work in **c** high wear and **d** low wear conditions

Table 2 Characteristic coefficients and exponents of wear behavior for NR nanocomposites in the presence of carbon black

Filler type	k	n	β	α
High wear				
Clay	7E−13	3.75	6E−19	10.23
Fiber	5E−17	8.27	9E−70	51.77
General	2E−15	6.58	3E−32	21.07
Low wear				
Clay	2E−30	20.30	3E−257	204.31
Fiber	1E−20	10.91	1E−41	27.88
General	9E−25	14.86	3E−65	47.33

to yield linear relationships in elastomeric microcomposites [27, 28].

The following power law equation describes the relationship between frictional work input per unit revolution and volume loss (V).

$$V = k \cdot F_w^n \quad (1)$$

while Eq. 2 depicts the relationship between normal load and volume loss.

$$V = \beta \cdot N^{\alpha} \quad (2)$$

where, normal load is designated as N, frictional work as F_w, and β, α, k, and n are constants, dependent on the nature of the abrader surface and the rubber.

The low wear state corresponds to unsteady or quasi-steady state abrasion. In accord with the above equations, this is also reflected in higher values of the exponents (n and α) when compared to those of the high wear (steady state) conditions (Table 2). In other words, the corresponding best fit lines in Fig. 3b and d have steeper slopes in the low wear conditions. The worn surfaces also bear marks of unsteady state of abrasion, as they exhibit a few microridges in between each macroridge (discussed later in Fig. 4j–l). Similar qualitative behavior was observed by Zhang [29] for conventional rubber composites, although quantitatively Zhang had reported lower absolute values of 'n' due to the use of different conditions. This highlights the difference in abrasion behavior in elastomeric macro- and nanocomposites. The other important observation emanating from Fig. 3 and Table 2 is that, here, both the coefficients and exponents are remarkably different (particularly under unsteady state condition) from those observed earlier in the nanocomposites devoid of CB [25]. In the compounds devoid of CB, the power law exponents were significantly lower (range from 0.2 to 2.6) and also the coefficients were somewhat larger (~E−17) [25].

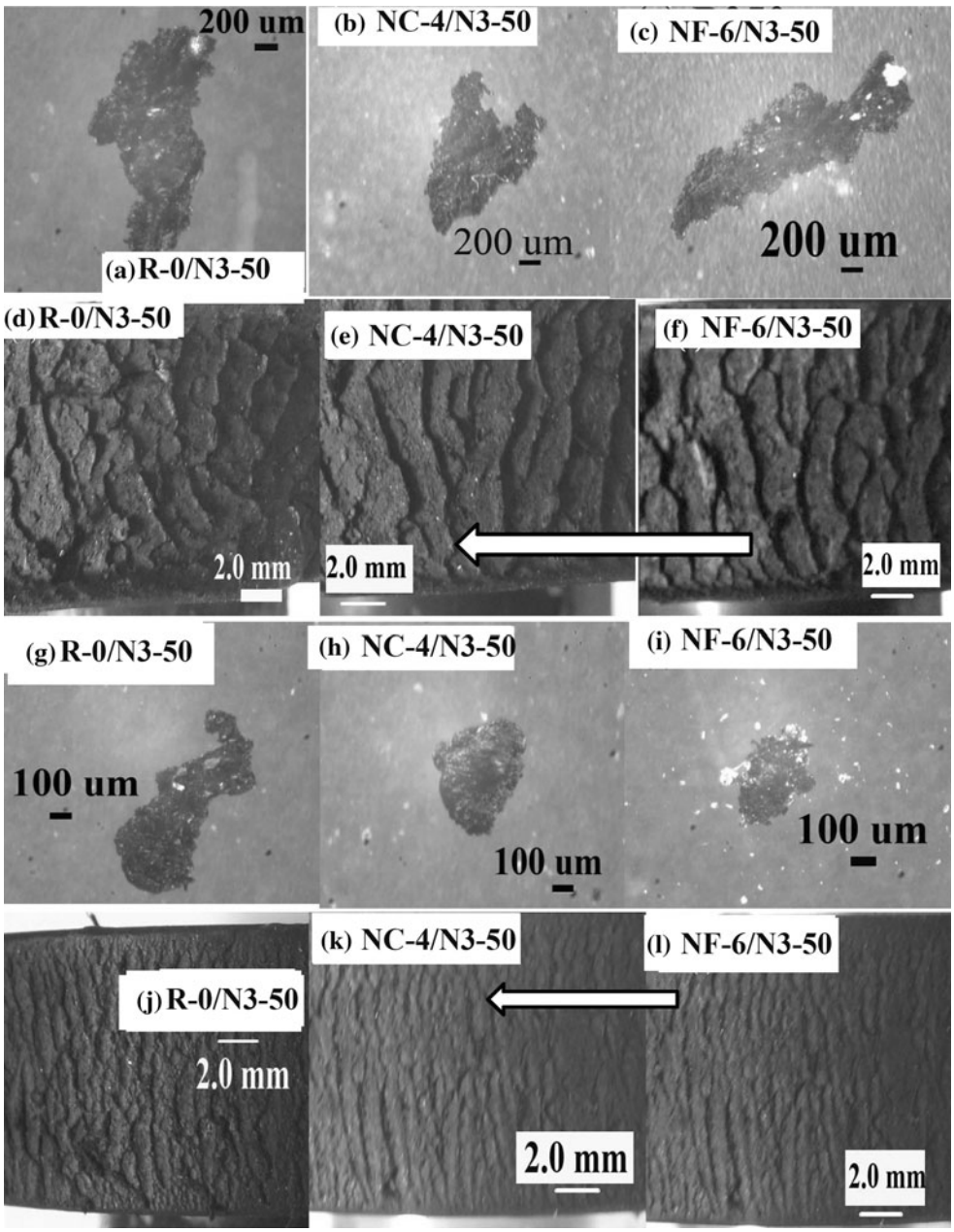

Fig. 4 Representative photomicrographs of the debris and the abraded surface produced during abrasion of carbon black filled NR nanocomposites (*arrows* indicate sliding direction)

Here, it is observed that the power law exponents are much higher as the best fit lines have steep slopes (Table 2; Fig. 3).

Table 3 displays the wear characteristics of the dual filler nanocomposites under the two sets of experimental conditions (high and low wear). In these CB filled compounds, the presence of CNF arrests wear behavior more than nanoclay, as reflected by the lesser wear loss generated (Table 3). The NF-6 based compounds arrest the wear more, however, they exhibit greater dependence on load (steeper slopes than clay and the average in Fig. 3a, c) in the high severity conditions. This is also reflected in the large values of the exponents (n and α) in Table 2. In the high wear condition, in comparison to the control (R-0/N3-50), the clay based CB filled (50 phr) nanocomposites exhibit up to 56% reduction in wear volumes, while their CNF based counterparts register up to 75% reduction. The corresponding reductions over the gum (R-0) are 79 and 89%, respectively. Amongst other things, this is because of the formation of a thin carbon layer on the blade and

Table 3 Wear characteristics of NR nanoclay and CNF nanocomposites in presence of CB

Sample designation	Vol. loss × 10^6 (m^3)	COF	Temp diff. (°C)	Aggregate particle			Intrinsic particle		
				Feret Dmtr. (mm)	Area (mm^2)	Perim (mm)	Feret Dmtr. (mm)	Area (mm^2)	Perim (mm)
High wear									
NR	10.66	1.16	10	3.0	2.1	11.2	1.0	0.4	3.4
R-0/N3-50	5.04	1.18	11	2.8	2.1	11.0	1.1	0.4	4.7
NC-4/N3-30	2.59	0.96	3	1.9	0.9	8.4	1.2	0.4	3.9
NC-4/N3-40	2.51	0.95	5	1.5	0.8	7.4	1.1	0.3	3.7
NC-4/N3-50	2.22	0.93	7	1.5	0.6	5.3	0.9	0.3	3.0
NF-6/N3-30	2.19	0.93	3	2.2	0.9	8.0	1.2	0.4	3.6
NF-6/N3-40	1.76	0.91	4	1.5	0.7	6.4	0.9	0.3	3.3
NF-6/N3-50	1.26	0.90	5	1.4	0.5	5.0	0.8	0.3	2.8
Low wear									
NR	0.58	1.26	1	2.8	2.6	11.0	1.3	0.9	4.3
R-0/N3-50	0.15	1.19	1	1.8	1.4	8.1	0.8	0.7	3.8
NC-4/N3-30	0.25	1.25	1	1.9	0.9	9.9	1.4	0.6	4.1
NC-4/N3-40	0.21	1.24	1	1.6	0.8	9.6	1.4	0.6	4.0
NC-4/N3-50	0.14	1.19	2	2.1	0.7	7.1	1.1	0.5	3.9
NF-6/N3-30	0.15	1.19	1	1.7	0.7	8.6	0.8	0.5	4.1
NF-6/N3-40	0.14	1.16	1	1.6	0.6	7.8	0.7	0.4	3.8
NF-6/N3-50	0.11	1.11	1	1.5	0.5	6.2	0.9	0.3	3.0

improvement in thermal conductivity, which in turn reduces the coefficient of friction. The sliding of the hard counterface over the rubber results in material transfer onto the counterface surface which forms a thin film. Depending on the bonding strength of the film and the counterface, the soft shield reduces rubber wear. The increase in blade weight in spite of steel abrasion by rubber and the loss in the glossy nature of the blade surface testify the transfer of material. Similar transfer film formation has been recorded with short carbon fiber in epoxy matrix [30]. However, in the presence of dual filler systems, the microstructural development has the most significant bearing on the wear behavior, as discussed below.

The remarkable improvement in abrasion resistance (up to 75% over the only black microcomposite) in the presence of nanofillers in highly filled black samples is primarily due to the attainment of a unique ternary filler arrangement within the matrix [discussed in Part I, with the help of representative transmission electron micrographs and zeta potential (ZP) values]. Such black-nanofiller associations are rendered possible by the residence of nanofiller in close proximity of the spherical CB (often tangentially) because of favorable electrostatic interactions governed by their respective zeta potentials. ZP is a measure of surface charge and it must be noted here that in the pH levels prevalent in this matrix, the nanofillers would have negative zeta potential (ZP) [31, 32], while CB would have positive values for the same [33]. This has been discussed numerically in Part I of this series. ZP has been utilized here merely as a tool to represent the charges on the nanofillers which are otherwise difficult to measure real-time in such complicated elastomer systems. It must also be mentioned here that zeta potential is not only applicable to aqueous systems, but also to highly viscous non aqueous fluids like polymer melts. For instance, Brochard-Wyart and de Gennes [34] and Flores et al. [35] have studied ionic diffusion of ultrafine particles in polymer melts.

The beneficial effect of such zeta potential driven associations (nanoblocks) have earlier been illustrated [36–38], as they seminate the formation of two types of CB entities in the nanocomposites—one in close proximity of nanofiller (clay/nanofiber) and the other in aggregates of other CB particles. The former has been earlier referred to as "associated CB" and the latter as "free CB" [37]. The "associated CB" is analogous to the "nanoblocks" described here in this series (Scheme 2). The distribution of free CB in the presence of nanofillers leads to the formation of efficient networks because of the formation of "nanochannels". These channels are networks of free CB particles that connect the "nanoblocks" leading to pathways for efficient deflection of tear path, stress transfer, and heat dissipation.

Table 3 also highlights that the CB filled nanocomposites depict stronger wear resistant behavior under high wear than those under low wear conditions. In high wear state,

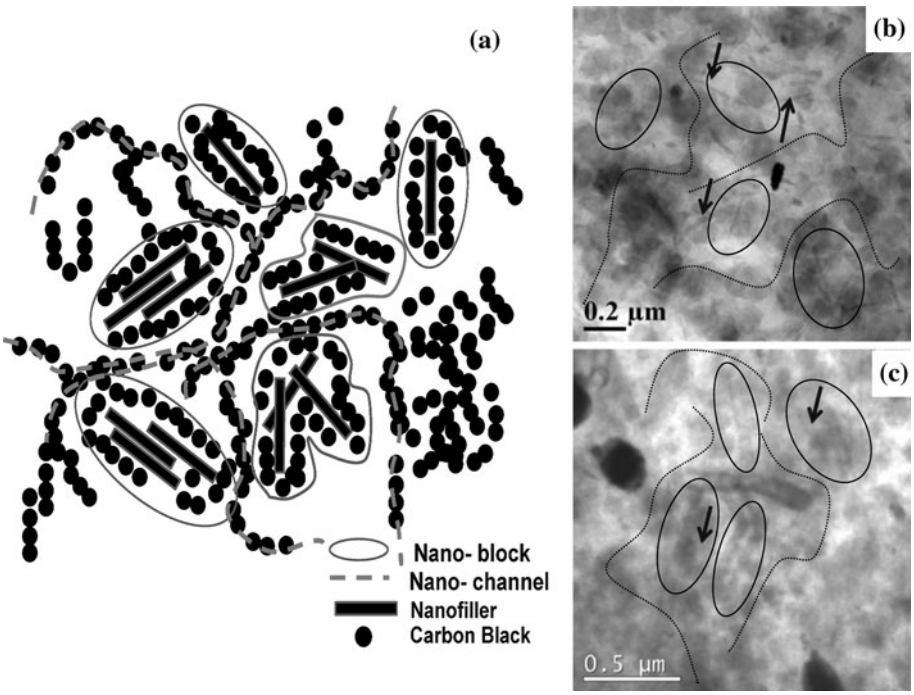

Scheme 2 Microstructural development in nanoclay and nanofiber based nanocomposites in the presence of CB: **a** schematic representation, and corresponding morphology in **b** nanoclay and **c** nanofiber based dual filler nanocomposites, as observed in transmission electron micrographs

these compounds have lower COF and temperature build-up (Table 3) than the CB filled clay based nanocomposites and the control microcomposite as well. Thus, they generate lower frictional work than other compounds at identical normal loading. The coefficient of friction of CB filled microcomposite (R-0/N3-50) is slightly higher than the gum; however, it is lowered by up to 26% with the addition of these nanofillers (Table 3). The lowering of coefficient of friction, as compared to that of the only black filled composite, plays the prominent role in reduction of frictional wear. At high severities, large amount of heat is generated, which needs to be dissipated. These CB filled nanocomposites are able to dissipate the stored energy, thereby reducing the wear volumes significantly, because of the establishment of a conducting network through the formation of the unique microstructure comprised of interconnected "nanoblocks" and "nanochannels" described above (Scheme 2). Such microstructures are also formed in the clay based nanocomposites, but nanoclay acts as heat sink thereby changing the heat dissipation pathway. This explains the stronger wear resistant behavior exhibited by the CNF based dual filler nanocomposites.

It is seen from Fig. 3 that at both high and low severities, the volume loss of the gum compound (R-0) is larger than those of the CB filled nanocomposites and the only CB microcomposite. Quantitatively NF-6 based compounds retain their advantage over the NC-4 based counterparts even as we traverse from steady state to transient state wear (low wear conditions in Table 3). It is of interest to note that this transition involves inversion of certain wear characteristics. First of all, unlike in high wear state, all the compounds demonstrate COF greater than unity under low wear condition. The COF, however, decreases with CB loading because of the formation of transfer film and also the development of the unique ternary microstructure described above. The role of oil and excess surfactant (which may act as a lubricant) during the wearing process is unclear and may contribute towards the lowering of coefficient of friction. This is also reflected in Fig. 3 (see *X*-axis values) as greater frictional work is generated in low wear condition employed than in the high wear state. Secondly, the control microcomposite exhibits lower wear than some of the CB-clay filled nanocomposites (Table 3; Fig. 3b, d). Finally, the order of the slopes of the best fit lines undergoes a visible change (Fig. 3b, d) in comparison to those in the high wear condition (Fig. 3a, c). CB filled nanocomposites based on NF-6 illustrate lesser load dependence than the NC-4 based systems as is clearly seen from the flatter slopes of the best fit lines. This implies that wear in the steady and unsteady states undertake different pathways and have different mechanisms.

At first look, this might appear a trifle counterintuitive. But, the wear processes, it must be remembered, are governed by different mechanisms. The differences in the strength and extensibilities play the dominant role at high severities, where frictional wear prevails; while at low severities, which correspond to the transient state of abrasion, the differences in crack growth rates and fatigue have been found to be the determining factors [27]. Bhowmick and co-workers [25, 28] had also found that at low loads

fatigue wear dominated, whereas at higher ones frictional wear was more prominent. Thus, the observed inversion in wear characteristics at low severities can be attributed to the fatigue behavior of these compounds.

The fatigue life (N) of strain crystallizing rubbers (like NR) is inversely related to the strain energy density (W), to be precise, $N \sim 1/W^2$ [39]. Since wear at low loads is fatigue dominated, the longer the fatigue life, the lower is the concomitant wear. As observed from the tensile properties reported in part I of this series, the NF-6 based compounds possess lower W ($\sim$18% less at 50 phr loading) than their clay based counter parts. Thus, NF-6 based CB filled compounds demonstrate longer fatigue life and lower wear than the NC-4 based compounds. This decrement in fatigue life of NC-4 based CB filled nanocomposites is because of the change in the conduction pathway in presence of clay, as the clay acts as a heat sink. This fall in fatigue life is thus associated with higher wear (compared to NF-6 based compounds) at low severities (Table 3; Fig. 3b, d).

The control microcomposite (R-0/N3-50), having low tensile strength (20 MPa) and high elongation at break (973%, discussed in part I of this series), exhibits strain energy density value marginally more than the corresponding NF-6 based compound. Since its W value is lower than those of the NC-4 based CB filled nanocomposites, it possesses longer fatigue life. This explains the fact why in low severity conditions R-0/N3-50 registers comparatively lower wear than some of the CB-clay filled nanocomposites. Thus, for the compounds having comparable tensile and tear strengths, the wear behavior in the transient state (low severity) is governed by the differences in their strain energy densities. This explains the peculiar inversion in wear characteristics while traversing from high to low wear domain.

Figure 4 displays the representative photomicrographs of the debris and the abraded surface produced. Two major type and size of debris are observed: (A) Aggregates (Fig. 4a–c) and (B) Intrinsic particles (Fig. 4g–i). Aggregate particles result in larger particles as they are generated from the periodic tearing away of tongues forming the characteristic abrasion pattern generated from the discontinuous waves of detachment [40]. On the other hand, intrinsic particles originate either from asperity induced microtearing or the growth of microflaws.

Cumulative abrasion leads to the eventual formation of the ridges by the process of detachment of the basic intrinsic particles. These ridges fold over on each passing of the abrader, thereby protecting the trailing edge (wake zone) from further wear by forming a tongue [40]. Champ et al. [41] have proposed that due to mechanical fatigue caused by repeated straining, the tongue tip tears away leading to formation of the larger debris, which in fact accounts for the major volume of the wear. In terms of the ridge formation, the nanofiller containing surfaces (Fig. 4e–f, k–l) are relatively smoother than the only black compounds (Fig. 4d, j), bearing proof of the low wear loss. Furthermore, it is observed that the volume loss became independent of the number of revolutions, and constancy in the distance between ridges too is established at high severity (Fig. 4d–f). Under low wear conditions, though the wear loss is low but volume loss is not strictly constant and microridges are still being formed (Fig. 4j–l). This also reflects that the wear dynamics and mechanisms, as discussed earlier, are different under low and severe wear conditions. These observations reaffirm the understanding that the high severity conditions correspond to steady state, whereas a transient state is established under the low severity conditions.

The synergy of fillers and the benefits of formation of "nanoblocks" and "nanochannels" are reflected in the restricted and less severe debris generation. This is so because ternary filler architecture and enhanced rubber-filler interaction causes the removal of fillers to be extremely unfavorable, resulting in less severe debris formation.

This is illustrated in Fig. 4 and Table 3, where it is seen that the average sizes of the characteristic bimodal distribution shifts towards smaller particles on incorporation of the nanofillers. The bimodal distribution is observed from the formation of aggregate and intrinsic particles, under both low and high wear conditions. The black filled compound, R-0/N3-50, forms aggregate debris of 11 mm perimeter, which progressively decreases through 8–5 mm as one moves from 30 to 50 phr black filled nanocomposites. The intrinsic particles, as seen earlier [25, 28], remain almost invariant. It may also be noted that the wear debris generated are at times known to act like a lubricant or third-body in reducing the wear rate by a rolling action [4].

The ploughing action of the blade causes the formation of the characteristic ridges on the abraded rubber surface (Fig. 4d–f, j–l), perpendicular to that of sliding direction of the abrader. In line with our earlier work [25], the ridge spacing is found to increase, although marginally, with increase in tan δ under both the conditions of high and low wear (Fig. 5a). Figure 5 details the influence exerted by the viscoelastic properties on the abrasion process in terms of the change in the ridge spacing. The effect is, however, less prominent than in the case of the gum nanocomposites observed earlier [25]. Here, the power law exponents are much lower, almost a third of those for NR nanocomposites devoid of CB. This signifies that there is reduction in the contribution of the viscous loss components towards the cumulative wear process.

In accord with the observations by Thavamani et al. [28], ridge spacing has been found to influence the

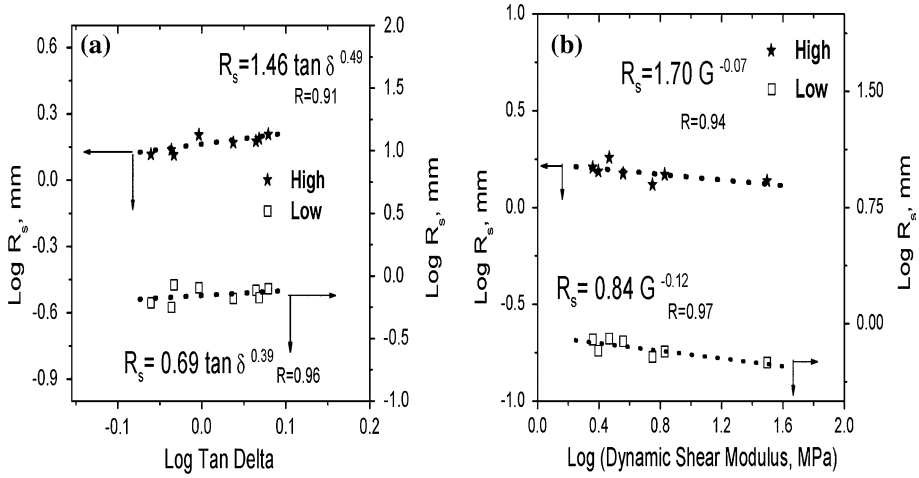

Fig. 5 Effect of viscoelastic properties **a** tan δ and **b** dynamic shear modulus on the ridge spacing

temperature development and volume loss, which is illustrated in Fig. 6. Figure 6a, b corresponds to the high and low wear conditions, respectively. Volume loss is known to increase with ridge spacing. It does so with increasing load as well (Fig. 3). Thus, close correspondence may be expected the effects of ridge spacing and load on the volume loss, under the two different sets of conditions employed here. A close look at the power law exponents generated by the best fit lines in Fig. 6 substantiates the above hypothesis. As in case of variation of load (Fig. 3), here as well, the exponent is much higher in the fatigue driven low wear condition than the friction dominated high severity condition (Fig. 6).

The wear behavior of these dual filler nanocomposites can thus be surmised to be better because of:

1. the propensity of forming a physical network structure of three dimensional nature,
2. haloing effect on nanofillers by CB resulting in the formation of "nanoblocks" and "nanochannels". Due to the presence of these channels, their concomitant filler network exhibits high thermal conductivity which results in significant reduction in the development of heat along with its fast dissipation, especially in the CNF based nanocomposites, and
3. the reduction in material loss, compared to conventional composites, because the rubber chain segments are of the same size as the surrounding nanofiller. It may be noted here that in conventional composites, filler aggregates are in the micrometer domain, as opposed to the nano domain prevalent here.

Rolling resistance and wet skid resistance

Elastomeric friction can be categorized mainly into two distinctive components—adhesion and hysteresis. Adhesive path leads to wear by roll formation driven by a strong surface phenomenon arising out of stick–slip action between the rubber and the abrader. Hysteresis leads to mild but continuous fatigue driven wear [42]. Thus, both these modes have viscoelasticity as the underlying principle. From earlier studies, it is known that the viscoelastic behavior of a rubbery material can be used for prognosis of its wear characteristic [22, 23]. Furthermore, the tan δ at very low temperatures (~ -60 °C) can be correlated with

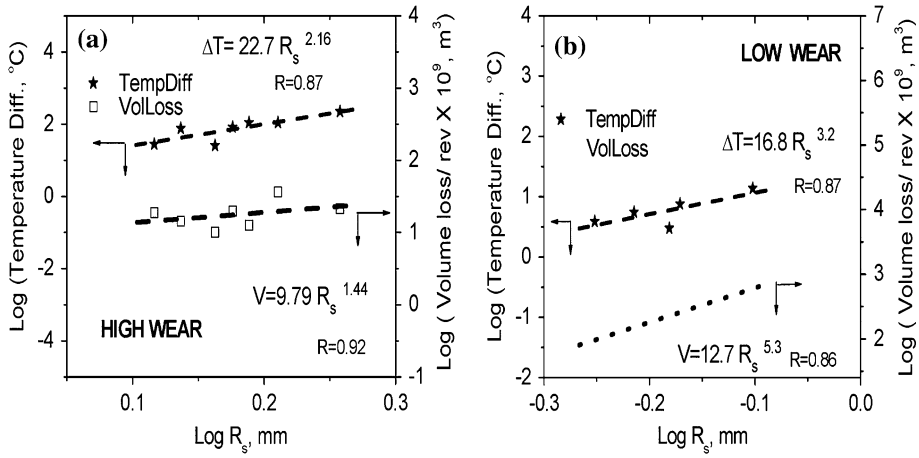

Fig. 6 Effect of ridge spacing temperature increase and volume loss in **a** high wear and **b** low wear studies

the abrasion resistance, while those at 0 and 60 °C correspond to the wet skid resistance and the rolling resistance in tire applications [43, 44]. It is desirable to have high loss factor at low temperatures (~−50 and 0 °C) to achieve necessary wear resistance and wet traction and grip. Considering the high frequency associated with the braking of tires, high viscous loss at low temperatures is considered to be beneficial for enhanced wet skid resistance of tires. Dynamic mechanical analysis was carried out across a wide temperature range for representative black filled clay and nanofiber nanocomposites under small-amplitude oscillatory tensile strain and the pertinent properties are reported in Table 4. The low temperature loss factor data corroborates the parallels between abrasion and viscoelastic behavior. The viscous loss data corresponding to rolling resistance illustrates the efficacy of these dual filler systems over the microcomposite (R-0/N3-50). All the dual filler containing systems possess lower tan δ at 60 °C. They exhibit reductions in the range of 6–34% over the control. The clay based nanocomposites provide marginally better performance in this regard (Table 4). Although these results have been discussed in detail in Part I of this series, a short recapitulation is provided here. Also, it has been reported earlier that if T_g is less than −60 °C, wet grip becomes inferior and, if it exceeds −40 °C, rolling resistance becomes inferior [45], all the compounds designed here lie within this high performance bracket (Table 4).

On using N330 black, a phenomenal increase of storage modulus (at 25 °C) is recorded in the presence of nanoclay over the only black filled control, for instance the 50 phr HAF filled sample, NC-4/N3-50, exhibits 326% increase (Table 4). The 50 phr CB loaded clay filled sample possibly shows the best mix of free and clay-aggregated CB leading to the formation of appropriate "nanochannels" for stress transfer (Table 4). The sepiolite clay acting as a dispersing agent for CB is able to form a network structure of small aggregates. This is reflected in terms of the superior mechanical properties (Part I of this series) and especially the remarkably high room temperature storage modulus (Table 4). As in the case of mechanical properties, with 130% increase, even the 40 phr CB loaded sample reflects the black-nanoclay synergy. Similar observations are made for the CNF containing black nanocomposites. The enhanced storage modulus would ensure dimensional stability during braking, driving and cornering of the tire.

The much enhanced properties in highly filled black samples are primarily due to the attainment of a unique ternary filler arrangement within the matrix, discussed in detail in Part I. The beneficial effect of such zeta potential driven associations (nanoblocks) provides the platform for efficient stress transfer, reduction in sub surface tearing and improved heat dissipation.

It can be clearly seen in Table 4, the clay-black nanocomposites, in particular, show the best mix of dynamic mechanical properties of high storage modulus, and tan δ at 0 °C along with significantly low rolling resistance.

Conclusions

1. In the presence of regular loadings of CB, both nanofillers lowered the wear characteristics of NR nanocomposites by virtue of black-nanofiller synergy. Improved abrasion resistance was observed not only at low severity conditions, but also that at high severity. Due to the enhanced efficacy of the heat dissipation pathway through the networks of "nanoblocks" and "nanochannels" CNF based nanocomposites were found to exhibit greater reduction in wear than their nanoclay counterparts.
2. The coefficient of friction of black filled composite was slightly higher than the gum. However, it was lowered by up to 26% with the addition of these nanofillers, due to the adherence of a transfer film onto the counterface surface. The volume loss (V) was related to the normal load (N) by the equation $V = \beta \cdot N^{\alpha}$ and with frictional work (F_w), by the

Table 4 Representative dynamic mechanical properties of NR gum and nanocomposites (both, nanoclay and nanofiber based) filled with HAF black at different loadings

Sample	T_g	tan δ_{max}	tan δ at 0 °C	tan δ at 60 °C	Storage mod. at 25 °C (MPa)	% Increase in modulus at 25 °C[a]
R-0/N3-50	−44	0.99	0.17	0.12	8.81	0
NC-4/N3-30	−50	1.16	0.10	0.08	10.84	23
NC-4/N3-40	−48	1.09	0.13	0.09	20.23	130
NC-4/N3-50	−50	0.92	0.10	0.09	37.49	326
NF-6/N3-30	−51	1.2	0.11	0.08	7.47	−15
NF-6/N3-40	−51	1.17	0.13	0.10	6.89	−22
NF-6/N3-50	−44	0.87	0.15	0.11	16.86	91

[a] % Increase over the control, R-0/N3-50

relation $V = k \cdot F_w^n$. The power law exponents are 3–4 times larger than those in the gum nanocomposites.

3. Abrasion followed stick–slip process and bimodal distribution of wear debris size was observed, resulting in the formation intrinsic and aggregated particles. While the intrinsic particles remain almost invariant, the aggregated particle size decreased significantly with CB loading in the nanocomposites causing reduction in material dissociation.
4. Characteristic abrasion patterns were formed on the surface of the abraded surface. It was seen that with ridge spacing, wear rate, and temperature build-up decreased with black-nanofiller synergy. As expected from common knowledge, wear parameters were decisively influenced by the viscoelastic properties of the nanocomposites. The wear rate and ridge spacing (R_s) were found to be related to the tan δ at T_g as power law functions.
5. The designed compounds lied within the high performance window of strong wet grip and low rolling resistance, while abrasion resistance improved stupendously.

References

1. Dasari A, Yu Z-Z, Mai Y-W, Hu GH, Varlet JL (2005) Compos Sci Technol 65:2314
2. Galetz MC, Blass T, Ruckdaschel H, Sandler JKW, Altstadt V, Glatzel U (2007) J Appl Polym Sci 104:4173
3. Karger-Kocsis J, Felhos D, Thomann R (2008) J Appl Polym Sci 108:724
4. Song J, Ehresntein GW (1993) In: Friedrich K (ed) Advances in composite tribology. Elsevier Science Publishers B.V., Amsterdam
5. Dasari A, Yu Z-Z, Mai Y-W (2009) Mater Sci Eng R 63:31
6. Donnet JB, Voet A (1976) Carbon black: physics, chemistry, and elastomer reinforcement. Dekker, New York
7. Maiti M, Bhattacharya M, Bhowmick AK (2008) Rubber Chem Technol 81:384
8. Chang L, Zhang Z, Ye L, Friedrich K (2007) Tribol Int 40:1170
9. Shi YJ, Feng X, Wang HY, Liu C, Lu XH (2007) Tribol Int 40:1195
10. Wang QH, Xu JF, Shen WC, Liu WM (1996) Wear 196:82
11. Li F, Hu K-A, Li J-L, Zhao B-Y (2001) Wear 249:877
12. Schadler LS, Laul KO, Smith RW, Petrovicova E (1997) J Therm Spray Technol 6:475
13. Bahadur S, Kapoor A (1992) Wear 155:49
14. Cai H, Yan FY, Xue QJ (2004) Mater Sci Eng A 364:94
15. Wang C, Dong B, Gao G-Y, Xu M-W, Li H-L (2008) Mater Sci Eng A 478:314
16. Zoo YS, An JW, Lim DP, Lim DS (2004) Tribol Lett 16:305
17. Ng CB, Schadler LS, Siegel RW (1999) Nanostruct Mater 12:507
18. Wetzel B, Haupert F, Friedrich K, Zhang MQ, Rong MZ (2002) Polym Eng Sci 42:1919
19. Shi G, Zhang MQ, Rong MZ, Wetzel B, Friedrich K (2003) Wear 254:784
20. Gatos KG, Kameo K, Karger-Kocsis J (2007) Express Polym Lett 1:27
21. Xu D, Karger-Kocsis J, Major Z, Thomann R (2009) J Appl Polym Sci 112:1461
22. Gent AN, Lai S-M, Nah C, Wang CHI (1994) Rubber Chem Technol 67:610
23. Maeda K, Bismarck A, Briscoe BJ (2005) Wear 259:651
24. Nayek S, Bhowmick AK, Pal SK, Chandra AK (2005) Rubber ChemTechnol 78:705
25. Bhattacharya M, Bhowmick AK (2010) Wear 269:152
26. Fukahori Y, Yamazaki H (1994) Wear 171:195
27. Gent AN, Pulford CTR (1983) J Appl Polym Sci 28:943
28. Thavamani P, Khastgir D, Bhowmick AK (1993) J Mater Sci 28:6318. doi:10.1007/BF01352190
29. Zhang SW (1984) Rubber Chem Technol 57:755
30. Bonfield W, Edwards BC, Markham AJ, White JR (1976) Wear 37:113
31. Kvandea I, Øyeb G, Hammera N, Rønninga M, Raaenc S, Holmena A, Sjöblomb J, Chen D (2008) Carbon 46:759
32. Gates WP (2004) Appl Clay Sci 27:1
33. Lin JJ, Chu CC, Chiang ML, Tsai WC (2006) J Phys Chem B110(37):18115
34. Brochard-Wyart F, de Gennes PG (2000) Eur Phys J E 1:93
35. Flores F, Graebling D, Allal A, Guerret-Pi′ecourt C (2007) J Phys D Appl Phys 40:2911
36. Konishi Y, Cakmak M (2005) Polymer 46:4811
37. Etika KC, Liu L, Hess LA, Grunlan JC (2009) Carbon 47:3128
38. Feller JF, Bruzaud S, Grohens Y (2004) Mater Lett 58:739
39. Gent AN (2005) In: Mark JE, Erman B, Eirich FR (eds) The science and technology of rubbers, 3rd edn. Elsevier Academic Press, San Diego, pp 455
40. Schallamach A (1954) Proc Phys Soc B67:883
41. Champ DH, Southern E, Thomas AG (1974) Am Chem Soc Div Org Coat Plast Paper Prepr 34:237
42. Moore D (1980) Wear 61:273
43. Gatti LF (2005) US Patent no. US 6852,785B1, Assigned to Dunlop Tire Corp., NY
44. Wang M-J, Morris MD (2008) In: Bhowmick AK (ed) Current topics in elastomer research. CRC Press, New York
45. Yuichi S, Susumu W, Sumio T (1992) European Patent no. EP0500338 (A1), Assigned to Sumitomo Rubber Ind